Geological Quarterly, 2024, 68: 17
DOI: http://dx.doi.org/10.7306/gq.1745

Long-term subsidence over the Upper Silesia Coal Basin identified on differential LIDAR (2012–2021) and InSAR (2015–2020) data

Maria PRZYŁUCKA[1, *], Zbigniew PERSKI[2] and Zbigniew KOWALSKI[1]

[1] Polish Geological Institute – National Research Institute, Rakowiecka 4, 00-975 Warszawa, Poland; ORCID: 0000-0002-2998-6008 [M.P.], 0000-0001-9229-2298 [Z.K.]

[2] Polish Geological Institute – National Research Institute, Skrzatów 1, 31-560 Kraków, Poland; ORCID: 0000-0002-6727-7448 [Z.P.]

Przyłucka, M., Prski, Z., Kowalski, Z., 2024. Long-term subsidence over the Upper Silesia Coal Basin identified on differential LIDAR (2012–2021) and InSAR (2015–2020) data. Geological Quarterly, 68: 11; https://doi.org/10.7306/gq.1745

Associate Editor: Piotr Krzywiec

We provide a map of subsidence caused by underground mining in Upper Silesia, which hosts the largest coal basin in Poland. The map combines data obtained using two InSAR processing techniques and differential LIDAR data. Persistent Scatterer Interferometry and Differential SAR Interferometry techniques were applied on images from the Sentinel-1 satellite covering a six-year period from 2015 to 2020. As a result, 132 subsidence areas affected by deformation of >5 mm/year covering 430 km^2 were determined. Additionally, a differential LIDAR model covering the period 2012–2021 was analyzed, where 103 subsidence areas were identified, of a total area of 88 km^2 and where the largest recorded deformation value exceeded 10 m. Despite the large time difference between the two subsidence datasets, good correlation of the data regarding the location and shape of the troughs was observed. However, comparison of InSAR and LIDAR data showed a large underestimation by DInSAR of values of subsidence in the central parts of the basins. We show the potential of Sentinel-1 and LIDAR data to determine displacements taking place over large areas and over long periods, as a supplement to traditional measurement methods.

Key words: DInSAR, InSAR, PSI, LIDAR, mining subsidence, Upper Silesia.

INTRODUCTION

INSAR METHODOLOGY

Interferometry comprises a group of techniques that uses the compound of two waves to obtain information about the change in the waveform. Satellite Radar Interferometry uses microwave imaging acquired by Synthetic Aperture Radar (SAR). The radar imaging system, in contrast to optical systems, allows penetration of clouds and is independent of sunlight (it can operate at night) and therefore is important for many Earth Observation applications. Each pixel of the radar image contains information about the amplitude and the phase of the signal reflected from the field unit. The combination of the phase compound of two SAR images of the same area is called an interferogram. The phase change recorded on the interferogram provides information on the change of distance between the satellite position and the field object on the Earth backscattering the signal. This allows the generation of a numerical terrain model and exact measurement of the surface displacements. The technique for creating differential interferograms is called differential SAR interferometry (DInSAR, Massonnet and Feigl, 1998). More about the technique's principles can be found for example in Hanssen (2001) or Ferretti et al. (2001).

The main limitations of differential interferometry include the de-correlation resulting from differences in time and geometry of obtaining two component images, the determination of phase ambiguity (phase unwrapping), and the estimation of atmospheric errors. Advanced processing, now called Persistent Scatterer Interferometry (PSI), initiated by Ferretti et al. (2000, 2001), overcomes these limitations. Thanks to the simultaneous processing of many scenes of the same area acquired at different times, atmospheric errors are reduced, and the value of relative deformation is determined with millimetric accuracy. This method is based on the analysis of pixels that have a good correlation and stable phases during a long period of time in the stack of interferograms. The result of the processing is a set of points, termed persistent scatterers (PS), to which are assigned the values of the average velocity of movement in the Line-Of-Sight (LOS) direction calculated in relation to the reference point, as well as a deformation time series with relative displacement values calculated for each image of the recording period. Consequently, the PSI technique supplements tradi-

* Corresponding author: e-mail: maria.przylucka@pgi.gov.pl

Received: September 12, 2023; accepted: March 23, 2024; first published online: April 30, 2024

tional DInSAR differential interferometry with data on very small displacements, of millimetres per year. The technique is widely used because of its ability to detect subtle, seemingly harmless, continuous deformation. Since 2000, many PSI processing algorithms have been developed (Crosetto et al., 2016; Wu et al., 2020; Raspini et al., 2022), differing in approaches to building individual interferograms and selecting their base configurations, PS points selection criteria and the deformation models used. The methods enable the detection of land surface changes with very high accuracy while ensuring extensive data coverage. As a result, they can extend traditional geodetic measurements and, in some cases, even replace them. The techniques are based on satellite data, so obtaining them does not require costly and time-consuming field research. At the same time, it is possible to study deformation that occurred in the past, thanks to the archiving of old scenes. The time of a satellite visit over a given area, from a few weeks to several days, allows for continuous monitoring and frequent supplementing of the research with new observations.

The InSAR processing techniques became very useful for the detection of ground surface movements related to such phenomena as earthquakes (e.g., Monterroso et al., 2020), volcanism (e.g., Poland and Zebker, 2020), mining subsidence (e.g., Herrera et al., 2010), landslides (e.g., Solari et al., 2020; Mondini et al., 2021), soil consolidation (e.g., Ramirez and Kwon, 2022) or other geohazards (e.g., Yun et al., 2020).

HISTORY OF INSAR SUBSIDENCE STUDIES OVER THE UPPER SILESIAN COAL BASIN

In areas where raw materials are mined underground, the greatest geohazards are associated with surface subsidence above the seams exploited. In mining areas, vertical terrain displacements are monitored using classical geodetic methods and occasionally using differential analyses of high-resolution numerical terrain models obtained by LIDAR. However, the main limitation of field-based geodetic monitoring techniques is the need for frequent field observations, which increases the monitoring costs. The monitored area is limited to two or three levelling lines directly in the impact area above the current production. Areas beyond those of greatest subsidence are not considered. In this context, the use of satellite data, which, if properly processed, can also help to identify terrain deformation, seems to be an ideal solution. It increases the frequency of a single measurement and supplements the data with areas not covered by levelling. Since the introduction of the method, Synthetic Aperture Radar Interferometry has proved to be very useful to track mining-induced ground deformation worldwide (e.g., Zhang et al., 2020; Modeste et al., 2021; Hu et al., 2023; Declercq et al., 2023). Also, the Upper Silesia Coal Basin (USCB) in Poland has been the subject of similar research since 1998 (Perski, 1998; Perski and Jura, 1999) and currently it is studied in several centres in Poland, e.g. by Ilieva et al. (2019), Pawłuszek-Filipiak and Borkowski (2020a), Sopata et al. (2020), Witkowski et al. (2021) and Dwornik et al. (2021). In PGI–NRI studies on InSAR ground deformation, monitoring of the USCB started with the Terrafirma project in 2005 (Graniczny et al., 2005) and over the years, a series of studies have been carried out (Graniczny et al., 2007, 2014; Czarnogórska, 2010; Del Ventisette et al., 2013) demonstrating the suitability of this method for this area. Further research focused on the advantages and disadvantages of using individual SAR sensors to monitor these geological processes (Przyłucka et al., 2014, 2015; Przyłucka and Graniczny, 2015; Graniczny et al., 2015; Przyłucka, 2017). The latest studies recognize the possibility of conducting long-term and large-scale analyses (Przyłucka et al., 2022). Among other things, it was found that the PS data from the C band made it possible to determine the boundary of the area influenced by mining activity but did not provide complete information on subsidence >30 mm per year. On the other hand, the greatest deformation is visible on traditional differential interferograms. Therefore DInSAR processing can supplement PSI results, although the different means of processing make combined analysis of the data difficult.

The launch of the European satellite Sentinel-1 in 2014 opened up entirely new possibilities. Access to free data with a time interval of 12 days (or even every 6 days for the full constellation Sentinel-1A/B, available to December 2021) now allows the analysis of data from the same sensor for several years of observation, and the combination of complementary (acquired from the same set of scenes) information from PSI and DInSAR processing. Our study addresses this particular theme.

LIDAR HIGH RESOLUTION DIGITAL ELEVATION MODELS

LIDAR (Light Detection and Ranging) is a remote sensing technique that utilises laser pulses to map the terrain, buildings and objects on the surface. A laser scanner located on board the aircraft collects information about the terrain during a single flight over the area. This technology finds various applications in such fields as geology, archaeology, spatial development and environmental protection (Liu, 2008). The undeniable advantage of this method is the large coverage of the measurements achieved in a short time. The absolute accuracy of the measurement is the sum of the accuracy of the scanning system, navigation and inertial data, assumptions and calibration of data blocks, and depends on the extent and the diversity of the relief and its vegetation cover. Typically, the height accuracy of the point cloud is in the range of 0.1 to 0.3 m, while the situational accuracy is in the range of 0.2 to 0.5 m. In mining, airborne laser scanning is used in, for instance, the analysis of ground surface subsidence, international examples of which can be found in the literature (e.g., Froese and Mei, 2008; Hu et al., 2022; Behera and Rawat, 2023). In the USCB, the results of the comparison of terrain height values between different time intervals and maps of subsidence basins for selected mining areas have been described, for example, in Polanin (2017). Currently, there is a trend in the Polish mining industry to perform photogrammetric flights in order to update the situational and height maps of the mining areas.

By opening access to the high-resolution LIDAR terrain model data covering the entire country, the Polish Head Office of Geodesy and Cartography made it possible to compare changes in the terrain surface for a period of 9 years (2012–2021) for the entire USCB. We describe the results obtained, focusing on subsidence troughs caused by underground coal mining, and compare them with InSAR results.

THE GOAL OF THIS STUDY

We show extensive and long-term subsidence, caused by underground mining and obtained from remote sensing data, covering an area of 5,600 km^2 of the USCB. Firstly, we describe results obtained from InSAR (DInSAR and PSI) processing of Sentinel-1 SAR data covering a period of 6 full years from 2015 to 2020. The analysis of traditional differential interferograms included the merge of the information obtained from 140 individual time intervals. The summed maps of the subsidence allowed assessment of the impact of coal mining activities and determination of the subsidence that occurred during 6 years across the entire area. Moreover, the preservation of individual

interferograms made it possible to analyse the development of individual troughs and increases in deformation in individual years. Furthermore, the PSI processing performed on 260 scenes from the same data path of the Sentinel-1 satellite resulted in obtaining over 10 million PS points, for which the average velocity of movement and time series of relative displacements were determined. The PS points allowed us to supplement the information on large-scale deformation with the residual movements occurring at the boundaries of the subsidence basins.

In the second part, the research focuses on differential LIDAR. The difference in the numerical models from 2021 and 2012 allowed for the identification of subsidence basins corresponding to a period of 9 years. Then, comparison between LIDAR and InSAR results on selected profiles of subsidence troughs is made. Finally, the advantages and disadvantages of the methodologies described are discussed.

STUDY AREA

The research area is located in the USCB, one of Europe's largest hard coal mining areas (Fig. 1). Administratively, the USCB is located within the Śląskie and Małopolskie voivodeships in Poland and the Czech Republic, and its area is estimated at 7,200 km^2, with 5,600 km^2 on the Polish part, which is the area of this study. As much as 30% of the entire basin is occupied by urbanized areas, forming the Upper Silesian Industrial District, the largest industrial district in Poland. The exploitation of hard coal started in the mid-17th century and significantly influenced the region's development. Currently, the basin's resources include 100 coal deposits, of which 81 still have current concession status (Szuflicki et al., 2022; Fig. 1).

The boundaries of the basin are determined based on the extent of Upper Carboniferous deposits and fault lines. In the west, the boundary is determined by folded Lower Carboniferous flysch deposits. In the north-east, the coal-bearing succession lies beneath Permian and Triassic deposits and above folded Lower Paleozoic rocks and Devonian and Lower Carboniferous strata. The southern boundary is erosive and is overlapped by Carpathian flysch (Chećko and Głogowska, 2010).

Mining activity began in the 17th century and continues to this day. Between 1945 and 1979, an average of 200 million tons of coal was mined annually (Konopko, 2010). Since the end of 1980, a steady decline resulted in a reduction in mining to 45 million tons of coal in 2020 (Szuflicki et al., 2022). Understandably, mining and industrial development was followed by urbanization, which now takes the form of 37 urban agglomerations (partly connected) and three million inhabitants.

Subsidence is one of the most significant threats related to underground mining. When the rock mass is disturbed by coal excavation, deformation and changes in stresses in the overburden occur, and as a result, displacements on the land surface arise. These can be immediate or long-term, related to consolidation and pressure dissipation in the rock. Subsidence can cause severe damage to buildings and infrastructure in the area. The effect of subsidence depends on many factors related to the type and amount of extraction, the type and size of buildings, as well as the rate of change itself. Subsidence resulting from underground coal mining with a longwall system and roof collapse follows the work front and is immediate.

However, the area potentially endangered by mining subsidence, i.e. the subsidence trough, is larger than the mining area. The boundary of this zone is determined by the extraction lead angle and the influence angle, which varies from 55 to 70° depending on the seam in use (Strozik, 2016). Mining subsidence in the USCB has been studied (e.g., Kowalski, 2015, 2020).

The two most frequently used mining systems in the area are a longwall system with a fall of the roof, and hydraulic backfill. The depression over a typical mining wall located at a depth of 680 m, 2.5 m high and 250 to 400 m long reaches up to 70% of the layer height, which corresponds to the most significant vertical displacement of 0.75–2.0 m in the central part of the basin (Dobak et al., 2009). Due to the exploitation of many seams, summed vertical displacements in the area can locally reach tens of metres. Mining work is usually concentrated on 3–4 faces per year so that the impact on the surface is as small as possible (Borecki, 1980).

In the USCB, the largest total displacement reaches 40 m. Klabis and Kowalski (2015) demonstrated subsidence basins in Bytom of up to 27 m in their geodetic measurements covering a period of 33 years of mining operations. It is estimated that over 600 km^2 is affected by vertical displacements (Kowalski, 2020). Even if the majority of these are agricultural and forest areas, terrain deformation also affects urban areas and contributes to the destruction of buildings and infrastructure.

METHODOLOGY

In the studies described, in order to determine mining-induced subsidence and to take full advantage of the potential of the Sentinel-1 data, a complex methodology was applied, consisting of separate processing of radar scenes using the classical differential interferometry technique and the PSI technique.

Previous studies have shown that satellite radar interferometry is suitable in the USCB as a complementary method of monitoring terrain surface displacement. To ensure that the final identified subsidence values are the most reliable, the information obtained at the PS points and on the differential interferograms should be analyzed jointly. Przyłucka et al. (2015) described this process applied to the Bytom city area, where the PS data showed residual subsidence on the edges of the forming trough. At the same time, the differential interferograms allowed the identification of significant changes occurring in its central part. Pawłuszek-Filipiak and Borkowski (2020b) also produced similar studies in the area of the Rydułtowy mine. The nature of the ground surface movements caused by underground coal mining in the USCB means that the PS points are not sufficient to identify the most significant displacement due to its highly non-linear behaviour over time. At the same time, residual displacements are not visible on the interferograms. Therefore, these two techniques complement each other and together allow for a complete description of the terrain changes.

An additional source of information on subsidence were LIDAR digital terrain models. The availability of new and archived data ensured full coverage of the research area and the identification of all subsidence basins formed over a period of 9 years.

PSI

This work used satellite scenes from the Sentinel-1 satellite descending path 124. In the PSI processing, a total of 260 scenes recorded at minimum intervals of 12 days (for one Sentinel-1 satellite) or every 6 days for the entire Sentinel-1 A / B constellation, covering the period 2014/10/26 – 2020/06/26, were used (Fig. 2). The resulting set includes 10,201,730 PS points over an area of 8,150 km^2, giving an average density of 1,252 PS/km^2. However, the occurrence of PS points is irregu-

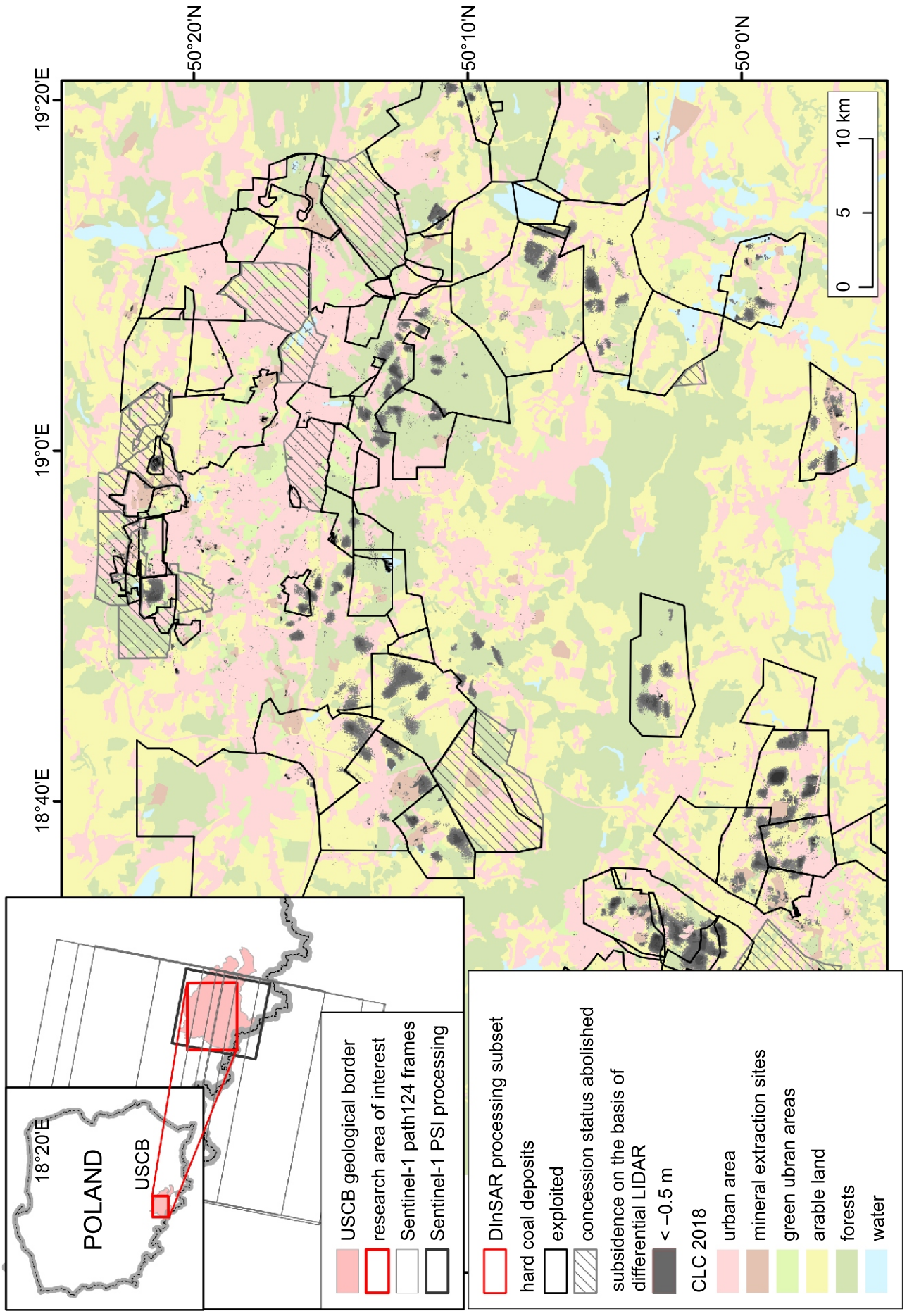

Fig. 1. The study area on a background of the Corine Land Cover 2018

The black polygons are the boundaries of hard coal deposits. The dark grey basin areas are subsidence locations determined on the basis of the LIDAR 2012-2021 differential terrain model. The red frames are subset areas used for DInSAR processing

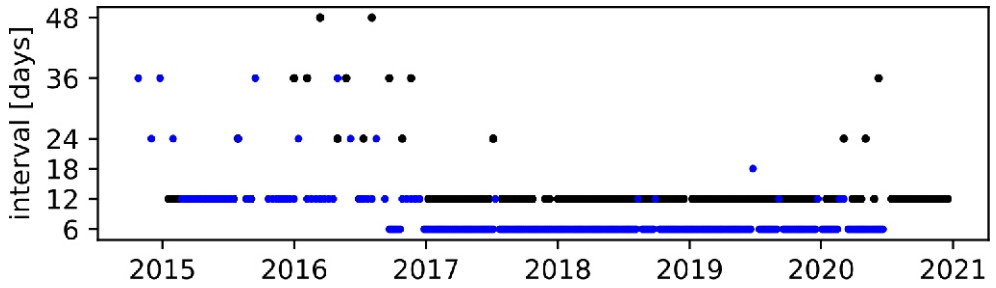

Fig. 2. Diagram of time intervals between successive Sentinel-1 SLC SAR scenes used for DInSAR (black) and PSI (blue) processing.

Table 1

Main characteristic of the InSAR datasets. The lower right part includes a histogram of PS point mean velocity values

Processing	PSI	DInSAR
Band	C	C
Wavelength	5.5 cm	5.5 cm
Incidence angle	29–36°	29–36°
Orbital path	124	124
Acquisition mode	Descending	Descending
Resolution of the image	5 × 20 m	5 × 20 m
Min. / Max. the time span between two acquisitions	6 / 36 days	12 / 48 days
Temporal span	2014/10/26–2020/06/26	2015/01/18–2020/12/29
Area cover	8 150 km²	4 207 km^2
No. SAR images	260	195
Displacement along LOS between two fringes on the interferogram		2.8 cm (Crossetto et al., 2016)
Max. theoretical velocity between neighbouring PS	42.6 cm/year (Crossetto et al., 2016)	NA
Reference image	29.08.2017	
No. of PSs	10,201,730	
Density of PS points	1252 [no./ km²]	
μ ± σ	−0.4 ±0.0 mm/year	
VEL_{MIN}/VEL_{MAX}	−123.9/+58.5 mm/year	
	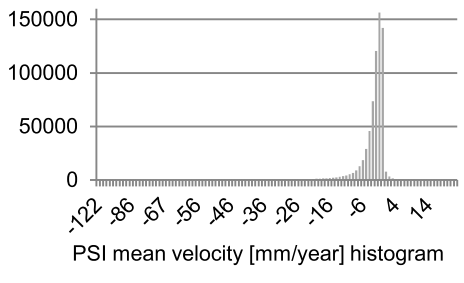 PSI mean velocity [mm/year] histogram	

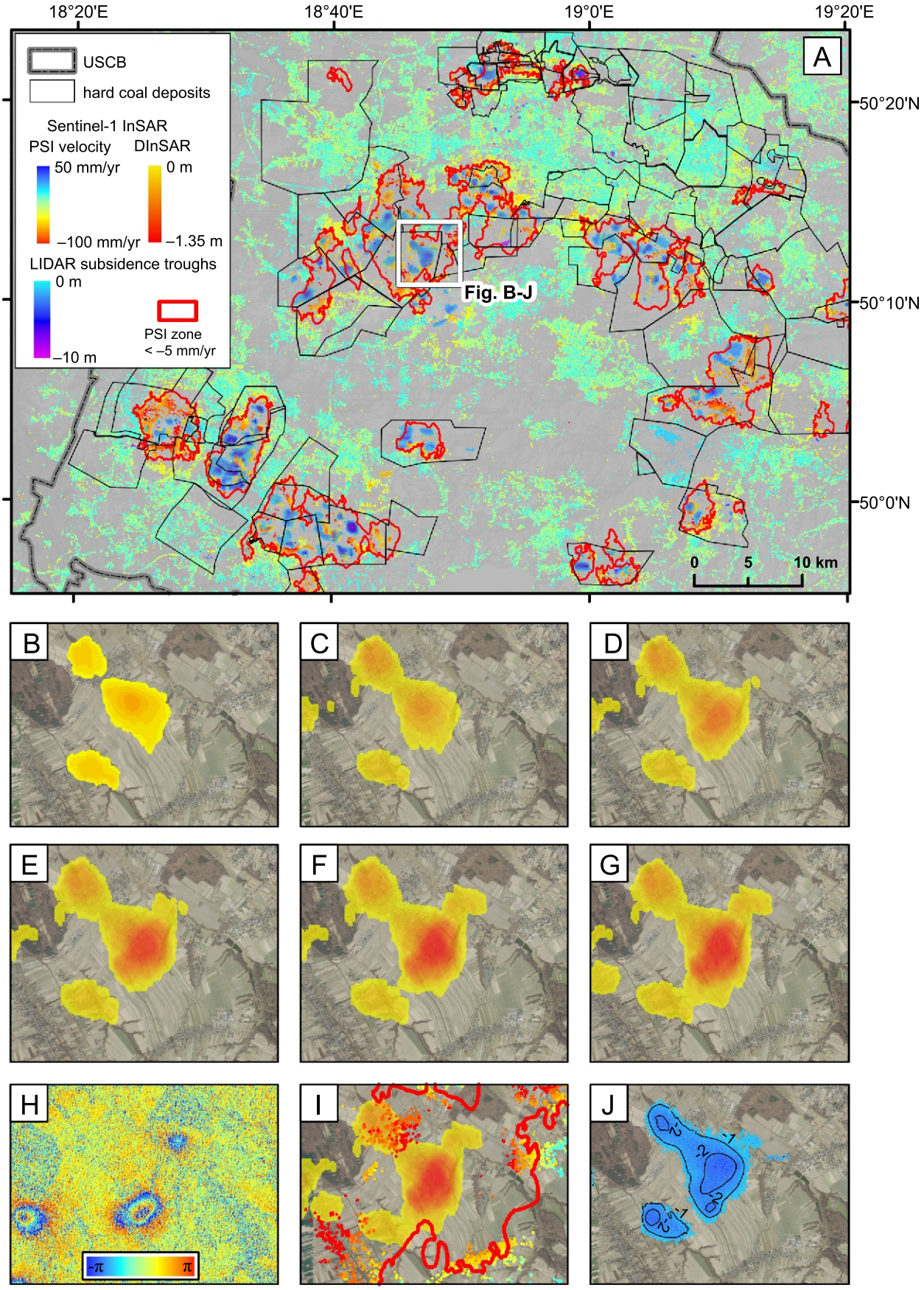

Fig. 3. InSAR processing and differential LIDAR results

A – PS point mean velocity in mm/year and DInSAR basin areas in a yellow-red colour scale. Differential LIDAR subsidence troughs in a blue-purple colour scale; **B**–**G** – subsidence on DInSAR results cumulatively with a one-year interval on the enlarged area of Ornontowice: (B) 2015, (C) 2015–2016, (D) 2015–2017, (E) 2015–2018, (F) 2015–2019, (G) 2015–2020; **H** – an example of one differential interferogram from Sentinel-1, dates 2020/02/21–2020/03/04, phase image in blue-red colour bar for radian values; I – PSI and DInSAR results plus zone of subsidence of more than –5 mm per year distinguished as red contour; **J** – differential LIDAR subsidence troughs on the enlarged area of Ornontowice with selected contours in metres

Table 2

Scheme of Sentinel-1 SLC SAR scene acquisition from descending path 124 for DInSAR processing for the study area with the number of interferogram time intervals

Year	Image coverage			Number of DInSAR time intervals
	South part of USCB	North part of USCB	Whole USCB	
2015	18	15	0	19
2016	6	6	5	11
2017	14	14	12	26
2018	8	8	22	30
2019	0	0	29	29
2020	0	0	25	25
sum	182			140

lar (Fig. 3). Their highest density is observed in urbanized areas and the lowest in forest areas. It should also be noted that there are no points for areas where the deformation rate is greater than 100 mm/year. Such areas are characterized by highly non-linear deformation in time, too much loss of coherence, which results in the rejection of PS points in the middle parts of the troughs by all processing algorithms. The processing was performed using Interferometric Toolbox Of PGI (InTOP) software (Perski et al., 2019).

DInSAR

For the DInSAR processing, 195 scenes were obtained, from which 182 differential interferograms were made, with time intervals of 12, 24, 36 or 48 days (Fig. 2). The dataset covers the period from 2015/01/18 to 2020/12/29: see Table 1 for basic characteristics of the dataset. For a significant number of data pairs, interferograms from one frame covered only part of the study area; therefore, it was necessary to make two interferograms from two different frames to cover the entire area (Table 2). The processing was performed using European Space Agency Sentinel Applications Platform (SNAP) software with the SNAPHU plugin, using both the GUI and SNAP command line Graph Processing Tool (gpt) as well as SNAP API from Python (snappy) tools. Trend elimination was performed in R software, raster merging in Global Mapper and other GIS analyses in ESRI ArcGIS. More detailed information on the processing steps realized is provided below.

The DInSAR processing methodology included classic processing of consecutive differential interferograms using single look complex (SLC) wide interferometric mode images in VV polarization. The Shuttle Radar Topography Mission (SRTM) 1 arc-sec (30 m resolution) DEM, provided by the US Geological Survey, was used to remove the topographic phase, and the Goldstein filter was applied.

Before phase unwrapping, in order to minimalize the atmospheric error effect, 12 subsets of the images were defined (Fig. 1). The subsets were selected to cover active mining areas where the most significant subsidence occurs, especially those not identified at the PS points. The following processing steps were performed separately for each subset. Phase unwrapping was done within the SNAPHU (Chen and Zebker, 2002) SNAP plugin with the MST initial method and DEFO statistical-cost mode. The unwrapped phase was then converted into displacement values (Phase to displacement tool) and geocoded with the Range Doppler Terrain Correction method. After that, the operator examined each resulting image to eliminate those for which the phase had not been unwrapped successfully. Subsequently, the subset's images from one calendar year were summed. Then, the elimination of the trend over the subsidence sum obtained was applied by fitting a second-order polynomial to subtract overlapping atmospheric errors.

In the last stage, images of the subsidence from one calendar year for an individual subset were combined, creating a deformation image for the entire research area. As a result, displacement images for each of the 6 years of observation were obtained. Finally, summing the images of the entire USCB allowed the final subsidence map for the period 2015/01–2020/12 to be produced (Fig. 3).

LIDAR

As a secondary source of information concerning long-term subsidence over the whole of Upper Silesia, a differential terrain model obtained from high-resolution LIDAR data was used. The differential model was created on the basis of two LIDAR models in a 1 m grid whose height accuracy is not less than 15 cm, representing the surface from 2012 and 2021 (Fig. 1). The models were made available by the Polish Head Office of Geodesy and Cartography. The resulting raster was resampled to a resolution of 20 m, close to the resolution of the final raster obtained from InSAR data. The differential model was created in *Global Mapper* software and further analyses were performed in ESRI ArcGIS.

RESULTS

The results obtained by PSI, DInSAR and differential LIDAR methods are shown in Figure 3. In particular, Figure 3A includes the subsidence basins identified and summed on InSAR interferograms covering a period of 6 years, and, superimposed on them, basins determined from the differential LIDAR model and PS points with additionally the value of the –5 mm per year deformation contour. The map also shows the boundaries of coal-mining areas. The methods shown successfully allowed the identification of places where ground surface deformation occurred in selected periods, although each method showed a different scale of usefulness in identifying individual values.

PSI RESULTS

The PSI processing of the Sentinel-1 A/B data resulted in 10 million PS measurement points. Each of these has several attributes, the most important being the mean velocity and the

time series of cumulated displacement value, which is relative to the master image, in this case in the middle of the time frame, i.e. 2017-08-29. The distribution of estimated displacements on PS, measured as an average velocity along satellite LOS during the whole time span, is shown in Figure 3A with a histogram and the main characteristics of the dataset in Table 1. The negative skewness in the LOS velocity histogram is explained by the dominant subsidence detected in the USCB. The mean standard deviation is nearly 0 mm/year.

It can be observed that the majority of PS points are placed in built-up areas, smaller and larger towns and on communication routes, while significant data gaps characterize forest and agricultural areas. Similarly, a lack of PS points is noticeable in the middle parts of the zones of cumulative subsidence, defined by mining areas. Although the highest observed velocity is as much as 120 mm/year (Table 1), most of the points where subsidence has been observed do not exceed 20 mm/year (see histogram in Table 1). Faster terrain movements cause a rejection of PS points due to decorrelation as described above.

The PS database made it possible to become acquainted with the scale of subsidence caused by underground mining, which took place over 6 years from 2015 to 2020. The PS points show similar changes in the terrain surface as published in other studies (Graniczny et al., 2015; Przyłucka et al., 2022), where data from other sensors were used. Undoubtedly, the broad coverage of the dataset and its high density enables us to draw preliminary conclusions regarding the entire area and individual mining sites. Firstly, it can be seen that despite the reduction in coal extraction in recent years, the area is still subject to significant change, and built-up areas are not free from the risk of subsidence. The lack of PS points in the central parts of the active mining areas suggests that the displacement there is very large. Subsidence has been observed over 65 out of 81 excavated hard coal deposits.

The PS points, after interpolation, form a surface of the average velocity of movements, which is easier to interpret than the point data. On the basis of the surface, zones within which subsidence of more than 5 mm/year occurs were designated (Fig. 3A). The total area of these zones is 430 km^2, of which 111 km^2 are built-up areas. Part of the subsidence falls outside the boundaries of the mining areas, specifically 68 km^2.

DINSAR RESULTS

Processing differential interferograms using the methodology described in the previous section resulted in the creation of a subsidence map for each year of observation separately. The successive sums of the areas obtained allowed the observation of subsidence cumulatively from 2015 to 2020, and the final image of the total displacements that occurred in 6 years. The DInSAR analysis allowed us to determine the maximum subsidence of up to 70 cm in one year and –1.35 m in the cumulated image of total measured displacement. In total, 132 basins with an area from 0.005 to 8.189 km^2 were observed, with a total area of 65.479 km^2, of which 11 km^2 are built-up areas (Fig. 3). Most of these occur within the boundaries of active mining areas in the period analysed. Some basins fall outside the areas of exploited deposits, similar to subsidence zones determined using the PSI technique. The small troughs identified outside the subsidence zones of the PS points can be considered phase unwrapping errors. As in the case of the PSI technique, coherence losses in vegetation-covered areas resulted in an incomplete picture of displacements in agricultural and forest areas. Also, manual analysis of individual interferograms after phase unwrapping revealed significant errors in obtaining reliable values.

Observation of the images of subsidence identified in subsequent years and the images of cumulative subsidence allows us to track the development of basins and changes in the boundaries of areas where the largest displacements occur. An example of the development of subsidence in the Ornontowice mining area is shown in Figure 3B–G. Each figure shows the accumulated subsidence at annual intervals. Figure 3G shows the total accumulated subsidence for the years 2015–2020, while Figure 3I additionally shows the residual velocities recorded at PSI points and the boundary of the area subject to deformation at –5 mm per year and Figure 3J the differential LIDAR results.

Often, where subsidence in the middle part of the troughs was large and fast, it was possible to notice at least two or even three interferometric fringes in the 12-day interval image, as seen on an example of the phase of a differential interferogram from the dates 2020/02/21–2020/03/04 in Figure 3H. In many cases, however, due to the irregularity in the coherence of individual pixels, it was not possible to properly unwrap the phase and, as a result, the values obtained were underestimated. The coverage of the displacement information was incomplete.

The troughs identified by DInSAR are located exactly in the zones designated by PS points (Fig. 3A). This corroborates the main assumptions of the analysis, i.e. determining the limits of the residual displacement based on PS data and supplementing it with the most significant deformation values using DInSAR. Also, it is clear that the total displacements on the maps obtained from DInSAR did not allow for determination of small, minor changes, which, however, were visible at PS points. This analysis leads to the conclusion that the more complete picture of deformation from the InSAR data in the USCB can be obtained only by combining information from two methods. At the same time, the nature of terrain surface changes and the presence of vegetation over a large part of the study area make us realize that even the combination of PSI and DInSAR results will not give a complete picture of the existing deformation.

From the analysis of the final image, it can be speculated that the total InSAR values are underestimates. Similar conclusions can be drawn by comparing the values obtained with published values from geodetic measurements, for example, by Ilieva et al. (2019) and Kowalski et al. (2021). Ilieva et al. (2019) showed 1 m of subsidence in the Miechowice area in Bytom city, which occurred only in half a year between April and October 2017, and Kowalski et al. (2021) described subsidence of nearly 2.2 m in Ruda Śląska for a three-year period between January 2018 and November 2020. Meanwhile, our map, which covers a more extended period, shows 0.31 and 0.81 m of deformation at these places, respectively.

Nevertheless, the analysis allows estimation of the scale of the subsidence that occurs in the study area. The locations of the troughs and their borders determined by residual subsidence are clearly associated with mining areas. The map allows us to identify areas where deformation occurs and compare these with topographic data.

DIFFERENTIAL LIDAR RESULTS

The differential terrain model was made by subtracting the surface from 2012 from the 2021 surface. To further compare the results with the InSAR image of ground subsidence, an analysis of the accuracy of the differential model was made. A single terrain surface model has a height accuracy of 15 cm, so it should be assumed that in the case of an unfavourable accumulation of errors of both models when creating their difference, the error may reach 30 cm. This was confirmed in the analysis

carried out in GIS on 204 selected points, where displacements during the period 2012–2021 should not occur, but the average value of the differential terrain model is 25 cm.

In order to select only those areas that correspond to subsidence troughs, the surface obtained from the differential model was replaced with contours. Taking into account the low accuracy of the differential terrain model (an error of up to 30 cm), contour lines with a value of –50 cm were considered as defining the boundaries of the subsidence troughs. From the set of places where subsidence occurred, segments with an area of <0.1 km^2 were removed as irrelevant. Based on the image of these contours, the subsidence troughs were cut out from the raster image of the differential terrain model. The resulting subsidence troughs so obtained were taken into account in further analyses.

In total 103 basins were identified, covering an area of 88 km^2. Locally, the difference in height value reached up to -38 m; however, these significant, large values were associated with open pit mining or changes in land cover (e.g. road construction). The greatest value of deformation in the central part of the basin related to underground mining was –108 cm.

DISCUSSION

Many studies have evaluated InSAR results for ground subsidence monitoring (e.g., Ferretti et al., 2007; Del Soldato et al., 2021), usually revealing a good quality of the processing results for small areas. In most cases, comparison with geodetic data, traditional levelling or GNSS measurements showed a good agreement of the deformation values obtained. As already discussed in previous sections, it has also been shown that within the USCB, the PSI technique fails to estimate large deformation values in the central part of the subsidence troughs due to their magnitude and a nonlinear mechanism. At the same time, it was also widely noted in previous publications that the DInSAR method, although it is able to detect high rates of subsidence, cannot provide very accurate measurements due to atmospheric limitations. However, most studies which have focused on determining the quality of InSAR results were based on short periods, several months or a year, and small study areas, e.g. one mining area or even single basins. The use of cumulative DInSAR processing results for six years of observations covering an area of five thousand km^2 decreases the accuracy of individual obtained values because the errors obtained on each interferogram are summed. The underestimation of large-scale deformation in the middle parts of the troughs resulting from phase unwrapping errors during a short period would not be as visible as following summing over the entire period. In turn, the most reliable value obtained as a result of PSI processing is not the deformation value (as is the case in geodetic measurements) but the average velocity value of the point.

The results obtained from the InSAR data were compared with the differential LIDAR terrain model between 2012 and 2021. The comparison with LIDAR data is less accurate than with the levelling data, but it allows us to evaluate the results obtained for the entire survey area.

The accuracy and quality of the resulting subsidence map from InSAR measurements were assessed in two stages. First, a qualitative assessment was performed, consisting of a visual interpretation of the differences between the two deformation images (Fig. 4). The following conclusions can be drawn: subsidence basin maps show a good correlation in terms of identifying the occurrence of deformation. The places of occurrence of the troughs coincide and are closely related to active mining areas. Nevertheless, as many as 48 places were not detected on the InSAR map, where subsidence exceeds 0.5 m on the differential LIDAR model. The total area of basins not identified in satellite data is 17.9 km^2. The analysis of these places, together with the CLC2018 land cover data, showed that these basins occur mainly in areas covered by vegetation and agricultural crops, and the places located in urbanised areas were small polygons (the average area of the polygon in urbanised areas within these basins was <0.05 km^2). These are the reasons for the occurrence of low coherence on the SAR data pixels, which made it difficult to detect the deformation. At the same time, although the DInSAR data did not detect large-scale subsidence visible on the differential model, 38 out of 48 of these polygons lie within the zones of residual subsidence determined based on PS data.

In the second validation stage, a quantitative comparison of the values on both maps was performed in two steps. First, 7984 points were generated in a 500 m regular grid covering the area of interest. The difference between the values of the final InSAR surface of deformation and the differential LIDAR model was calculated for each point. The root mean square of the differences between the values obtained at the points was used to calculate the Root-Mean-Square-Error (RMSE). This error amounted to 1.26 m. In the second step, 43 linear profiles passing through the subsidence basins were plotted on the map (Fig. 4). These profiles were drawn manually, and it was up to the operator to locate the profile so that it passed through the centre of the basin and intersected the area where the displacements were recorded. On each profile, points were determined every 20 m, with a total number of 7330 points. The difference between the values on the two surfaces obtained (InSAR and differential LIDAR) was determined for each point, and the RMSE error was recalculated based on these differences. This error amounted to 1.86 m.

The fourty three designated profiles were also used to visually compare the most critical places in terms of deformation recorded based on two measurement methods. Selected profiles are shown in Figure 5. Visualization of cross-sections in the vertical plane further highlighted the differences in the values. While the shape and location of the deformation more or less match, as also shown in the horizontal map in Figure 4, the underestimation in the InSAR data in many cases exceeds 1 m (as calculated by the RMSE error). Even considering the error of the differential LIDAR model (0.3 m), the comparison value obtained of the InSAR map is significant. This can be explained partly by the fact that the two maps cover different periods (the LIDAR model covers 9 years, whereas the InSAR map 6 years exactly in the middle of the LIDAR period). Nevertheless, such a sizeable mean error of the values obtained confirms the assumptions presented at the beginning of this section, that the resulting InSAR subsidence map cannot be treated as a map of accurate, reliable deformation values but only as an approximate image of them. On the other hand, the differential LIDAR model contains noise and incorrect values within a few tens of centimetres, which make it impossible to identify very small displacements and correctly assess the boundaries of the basins visible on the map of PSI points.

CONCLUSIONS

We have analysed PSI and DInSAR processing results together with a differential LIDAR model in order to create an integrated map of subsidence over the USCB. In order to ensure coverage of the entire coal basin, Sentinel-1 SLC SAR scenes of descending path 124 were used. 260 scenes from the period 2014/10/26–2020/06/26, processed with the PSI technique,

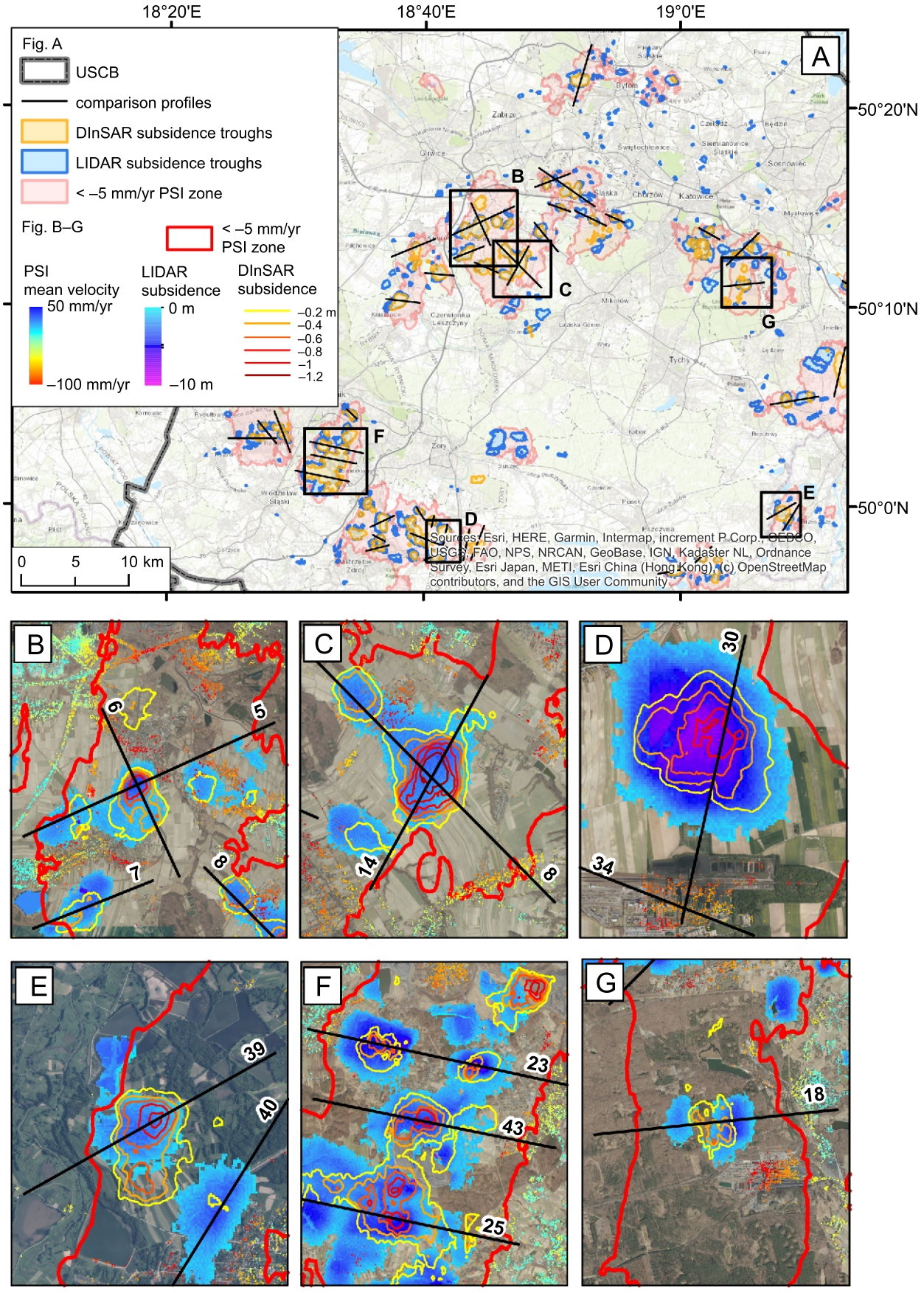

Fig. 4A – comparison of subsidence identified by DInSAR (yellow polygons), differential LIDAR (blue polygons) and PSI processing (pink polygons). The profiles used for the comparison of the differential LIDAR model and InSAR map are shown as black lines. B–G – enlargement of areas of selected profiles for graphs on Figure 5 (marked with numbers) with subsidence results from DInSAR (red-yellow contours), differential LIDAR (blue-purple raster) and PSI (blue-red points with red –5 mm/year contour)

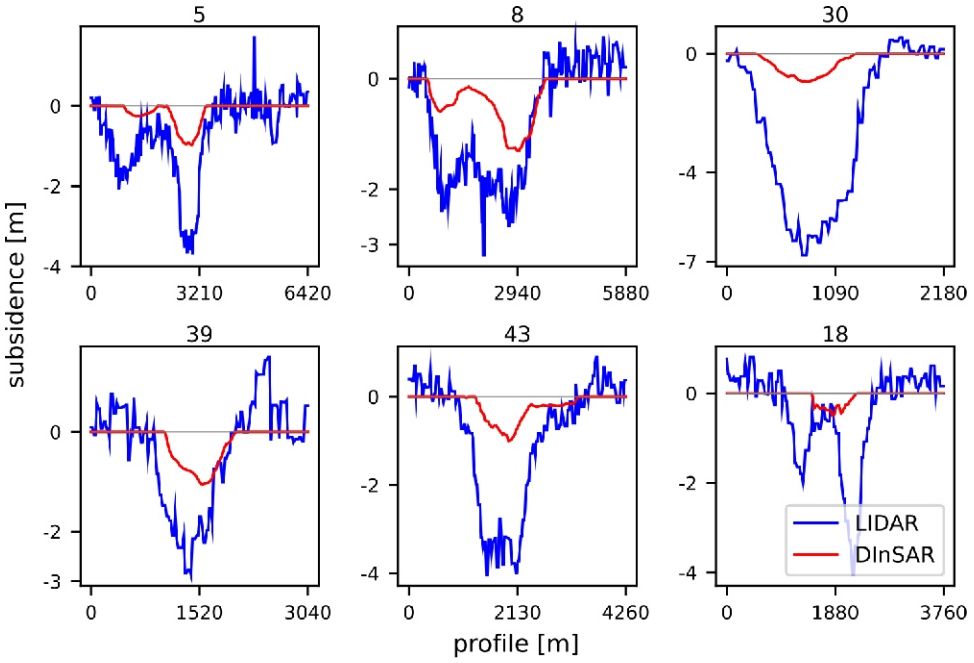

Fig. 5. Sections through the differential LIDAR model and DInSAR results on selected linear profiles (location of profiles in Fig. 4)

formed a database of average velocities with a mean density of 1252 PS/km^2. Next, 195 scenes were processed with the DInSAR technique, supplementing the subsidence information with 182 differential interferograms, covering the period 2015/01/18–2020/12/29. From these two processes, summary maps of subsidence were created: residual (the average velocity of PS points) and significant deformation (by summing the displacement revealed on the interferograms). To take full advantage of the Sentinel-1 data, these maps were combined into one, creating an integrated subsidence map for the entire USCB, covering six years. This map provides a picture of both major and minor subsidence. Based on these results, 132 areas of subsidence troughs were determined and 430 km^2 are affected by deformation greater than 5 mm per year. The highest observed value of subsidence was 1.35 m.

Additionally, a differential terrain model obtained from high-resolution LIDAR from 2021 and 2012 enabled the identification of deformation that occurred over a period of 9 years. LIDAR results showed 103 places where underground mining-induced land surface changes reached >10 m and in total covered an area of almost 90 km^2.

Comparison between InSAR and the differential LIDAR data allowed determination of the InSAR accuracy of the values obtained as low, of the order of several tens of centimetres, but in a reliable and comprehensive manner showing the overall picture of change in the terrain surface caused by long-term mining activity. In addition, the analysis of individual deformation surfaces obtained from the sum of differential interferograms in the annual periods made it possible to analyse the development of individual basins and to track increments of subsidence.

InSAR processing, like any measurement method, is not free from weaknesses. The lack of data in low coherence areas, errors associated with atmosphere influence and difficulties in phase unwrapping result in a low accuracy of the final values, especially over such a long period. Complex analysis of the results of two types of processing covering the area of the entire coal basin, the largest in Poland, made it possible to determine subsidence troughs and describe the scale and range of deformation in recent years,. In addition, they ensured the creation of a map covering a very long period of six years of observations. However, the comparison with the differential LIDAR terrain model showed a very large underestimation of the data in the central parts of the basins, described by an RMSE error of 1.86 m. On the other hand, residual subsidence determined on the basis of PS points has not been measured on either DInSAR maps or the LIDAR differential model. The map of PS points allowed the determination of areas subject to subsidence of more than -5 mm per year and thus supplemented the information on large subsidence revealed by DInSAR and differential LIDAR.

In summary, the InSAR methodology described allows for coarse monitoring of mining-induced subsidence. Although the discrepancy between resulting InSAR deformation map and differential LIDAR data clearly shows that in this specific case InSAR data are ineffective for operational use, USCB is one of the few areas in the world where, due to unique style of deformation, InSAR techniques so far fail despite their very promising results. In order to properly monitor areas like the USCB we need longer wavelength SAR such as, e.g., the L-band system (which has higher coherence in vegetated areas and, due to the longer wavelength, can identify larger displacements without signal decorrelation in the middle parts of the basins) with long-term cover similar to Sentinel-1, and InSAR dedicated acquisition modes. The detection of subsidence caused by underground mining using differential LIDAR models has shown great potential. The submission of data covering a period of 9 years allowed the identification of all areas where large subsidence basins developed, even where vegetation prevented InSAR measurements. However, LIDAR data may not be available for short time intervals, and updating them over such a large area is very expensive. In order to monitor in detail, or to supplement information about successive deformation increments in shorter periods, it is reasonable to use DInSAR measurements.

Acknowledgements. This research was carried out as part of a project financed by the National Fund for Environmental Protection and Water Management of the Polish Geological Institute – National Research Institute “Interferometric Monitoring of the Polish Area (InMoTeP) – stage II”, contract number 343/2021 / Wn-07 / FG- go-dn / D.

REFERENCES

Behera, A., Rawat, K.S., 2023. A brief review paper on mining subsidence and its geo-environmental impact. Materials Today: Proceedings, **1**; https://doi.org/10.1016/j.matpr.2023.04.183

Borecki, M., 1980. Ochrona powierzchni przed szkodami górniczymi (in Polish). Wyd. Śląsk, Katowice.

Chećko, J., Głogowska, M., 2010. Evaluation of CO_2 storage location brine strata and coal seams in Upper Silesian Coal Basin (GZW) region (in Polish with English summary). Przegląd Górniczy, **66**: 97–102.

Chen, C.W., Zebker, H.A., 2002. Phase unwrapping for large SAR interferograms: Statistical segmentation and generalized network models. IEEE Transactions on Geoscience and Remote Sensing, **40**: 1709–1719; https://doi.org /10.1109/TGRS.2002.802453

Crosetto, M., Monserrat, O., Cuevas-González, M., Devanthéry, N., Crippa, B., 2016. Persistent scatterer interferometry: a review. ISPRS Journal of Photogrammetry and Remote Sensing, **115:** 78–89; https://doi.org/10.1016/j.isprsjprs.2015.10.011

Czarnogórska, M., 2010. Dynamics of Earth's surface movements in selected regions of the Upper Silesian Coal Basin based on satellite interferometry (in Polish with English summary). Ph.D. Thesis. Państwowy Instytut Geologiczny – Państwowy Instytut Badawczy, Warszawa.

Declercq, P.Y., Dusar, M., Pirard, E., Verbeurgt, J., Choopani, A., Devleeschouwer, X., 2023. Post mining ground deformations transition related to coal mines closure in the Campine Coal Basin, Belgium, evidenced by three decades of MT-InSAR data. Remote Sensing, **15:** 725; https://doi.org/10.3390/rs15030725

Del Ventisette, C., Ciampalini, A., Manunta, M., Calò, F., Paglia, L., Ardizzone, F., et al., 2013. Exploitation of large archives of ERS and ENVISAT C-band SAR data to characterize ground deformations. Remote Sensing, **5:** 3896–3917; https://doi.org/10.3390/rs5083896

Del Soldato, M., Confuorto, P., Bianchini, S., Sbarra, P., Casagli, N., 2021. Review of works combining GNSS and InSAR in Europe. Remote Sensing, **13**: 1684; https://doi.org/10.3390/rs13091684

Dobak, P., Drągowski, A., Frankowski, Z., Frolik, A., Kaczyński, R., Kotyrba, A., Pinińska, J., Rybicki, S., Woźniak, H., 2009. Zasady dokumentowania warunków geologiczno-inżynierskich dla celów likwidacji kopalń (in Polish). Polish Ministry of Enviroment, Warsaw, 12–14 (84). ISBN 978-83-60117-86-6; https://www.pgi.gov.pl/docman-tree-all/publikacje-2/ksiazki/naukowe-i-metodyczne/252-zasady-dokumentowania-warunkow-geologicznych-dla-celow-likwidacji-kopaln/file.html

Dwornik, M., Porzycka-Strzelczyk, S., Strzelczyk, J., Malik, H., Murdzek, R., Franczyk, A., Bała, J., 2021. Automatic detection of subsidence troughs in SAR interferograms using mathematical morphology. Energies, **14**: 7785; https://doi.org/10.3390/en14227785

Ferretti, A., Prati, C., Rocca, F., 2000. Nonlinear subsidence rate estimation using Permanent Scatterers in Differential SAR Interferometry. IEEE Transactions on Geoscience and Remote Sensing, **38:** 2202–2212; https://doi.org/10.1109/36.868878

Ferretti, A., Prati, C., Rocca, F., 2001. Permanent scatterers InSAR Interferometry. IEEE Transactions on Geoscience and Remote Sensing**, 39:** 8–20; https://doi.org/10.1109/36.898661

Ferretti, A., Savio, G., Barzaghi, R., Borghi, A., Musazzi, S., Novali, F., Prati, C., Rocca, F., 2007. Submillimeter accuracy of InSAR time series: experimental validation. IEEE Transactions on Geoscience and Remote Sensing, **45:** 1142–1153; https://doi.org/10.1109/TGRS.2007.894440

Froese, C.R., Mei, S., 2008. Mapping and monitoring coal mine subsidence using LiDAR and InSAR. GeoEdmonton, **8:** 1127–1133.

Graniczny, M., Kowalski, Z., Jureczka, J., Czarnogórska, M., 2005. Terrafirma project-monitoring of subsidence of northeastern part of the Upper Silesian coal basin. Polish Geological Institute Special Papers, **20:** 59–63.

Graniczny, M., Kowalski, Z., Leśniak, A., Czarnogórska, M., Piątkowska, A., 2007. Analysis of the PSI data from the Upper Silesia – SW Poland. The International Forum on Satellite EO and Geohazards, The International Geohazard Week 5–9 November 2007 ESA-ESRIN Frascati, Rome.

Graniczny, M., Kowalski, Z., Przyłucka, M., 2014. Observation of the Mining-Induced Surface Deformations Using C and L SAR Bands: The Upper Silesian Coal Basin (Poland) Case Study. Mathematics of Planet Earth, Springer, Berlin, Heidelberg: 249–255; https://doi.org/10.1007/978-3-642-32408-6_57

Graniczny, M., Colombo, D., Kowalski, Z., Przyłucka, M., Zdanowski, A., 2015. New results on ground deformation in the Upper Silesian Coal Basin (southern Poland) obtained during the DORIS Project (EU-FP 7). Pure and Applied Geophysics, **172**: 3029–3042; https://doi.org/10.1007/s00024-014-0908-6

Hanssen, R., 2001. Radar Interferometry: Data Interpretation and Error Analysis. Dordrecht, Holland, Kluwer Academic Publishers; https://doi.org/10.1007/0-306-47633-9

Herrera, G., Tomás, R., Vicente, F., Lopez-Sanchez, J.M., Mallorquí, J.J., Mulas, J., 2010. Mapping ground movements in open pit mining areas using differential SAR interferometry. International Journal of Rock Mechanics and Mining Sciences, **47**: 1114–1125; https://doi.org/10.1016/j.ijrmms.2010.07.006

Hu ,L., Navarro-Hernández, M., Liu, X., Tomás, R., Tang, X., Bru, G., Ezquerro, P., Zhang, Q., 2022. Analysis of regional large-gradient land subsidence in the Alto Guadalentín Basin (Spain) using open-access aerial LiDAR datasets. Remote Sensing of Environment, **280**: 113218; https://doi.org/10.1016/j.rse.2022.113218

Hu, L., Tomás, R., Tang, X., López, V., Herrera, G., Li T., Liu Z., 2023. Updating Active deformation inventory maps in mining areas by integrating InSAR and LiDAR datasets. Remote Sensing**, 15**: 996; https://doi.org/10.3390/rs15040996

Ilieva, M., Polanin, P., Borkowski, A., Gruchlik, P., Smolak, K., Kowalski, A., Rohm, W., 2019. Mining deformation life cycle in the light of InSAR and deformation models. Remote Sensing, **11**: 745; https://doi.org/10.3390/rs11070745

Klabis, L., Kowalski, A., 2015. Mining exploitation in safety pillar for the city center of Bytom, history and the present (in Polish with English summary). Przegląd Górniczy, **71**: 33–43.

Konopko, W., 2010. Coal mining and rock mass destruction in the Upper Silesian Coal Basin (in Polish with English summary). Przegląd Górniczy, **66**: 1–10.

Kowalski, A., 2015. Deformacje powierzchni w Górnośląskim Zagłębiu Węglowym (in Polish). Wydawnictwo Głównego Instytutu Górnictwa, Katowice.

Kowalski, A., 2020. Deformacje powierzchni na terenach górniczych kopalni węgla kamiennego (in Polish). GIG, 2020, Katowice. ISBN: 978-83-65-50323-7.

Kowalski, A., Gruchlik, P., Polanin, P., Kiełbiowski, K., Rutkowski, T., 2021. Mining extraction in Ruda Śląska –Wirek, deformations and protection of the church building (in Polish with English summary). Przegląd Górniczy, **77:** 16–35.

Liu, X. 2008. Airborne LiDAR for DEM generation: some critical issues. Progress in physical geography, **32**: 31–49; https://doi.org/10.1177/0309133308089496

Massonnet, D., Feigl, K.L., 1998. Radar interferometry and its applications to changes in the earth's surface. Reviews of Geophysics, **36**: 441–500; https://doi.org/10.1029/97RG03139

Modeste, G., Doubre, C., Masson, F., 2021. Time evolution of mining-related residual subsidence monitored over a 24-year period using InSAR in southern Alsace, France. International Journal of Applied Earth Observation and Geoinformation, **102**: 102392; https://doi.org/10.1016/j.jag.2021.102392

Mondini, A.C., Guzzetti, F., Chang, K.T., Monserrat, O., Martha, T.R., Manconi, A., 2021. Landslide failures detection and mapping using Synthetic Aperture Radar: Past, present and future. Earth-Science Reviews, **216**: 103574; https://doi.org/10.1016/j.earscirev.2021.103574

Monterroso, F., Bonano, M., Luca, C.D., Lanari, R., Manunta, M., Manzo, M., Onorato, G., Zinno, I., Casu, F., 2020. A global archive of coseismic DInSAR products obtained through unsupervised Sentinel-1 data processing. Remote Sensing, **12**: 3189; https://doi.org/10.3390/rs12193189

Pawłuszek-Filipiak, K., Borkowski, A., 2020a. Comparison of PSI and DInSAR approach for the subsidence monitoring caused by coal mining exploitation. The International Archives of Photogrammetry, Remote Sensing and Spatial Information Sciences, **43**: 333–337; https://doi.org/10.5194/isprs-archives-XLIII-B3-2020-333-2020

Pawłuszek-Filipiak, K., Borkowski, A., 2020b. Integration of DInSAR and SBAS techniques to determine mining-related deformations using Sentinel-1 data: the case study of Rydułtowy mine in Poland. Remote Sensing, **12**: 242; https://doi.org/10.3390/rs12020242

Perski, Z., 1998. Applicability of ERS-1 and ERS-2 InSAR for land subsidence monitoring in the Silesian coal-mining region, Poland. International Archives of Photogrammetry and Remote Sensing, **32**: 555–558.

Perski, Z., Jura, D., 1999. ERS SAR interferometry for land subsidence detection in coal mining areas. Earth Observation Quarterly, **63**: 25–29.

Perski, Z., Brzeziński, M., Przyłucka, M., Pacanowski, G., Musiatewicz, M., Nowacki, Ł., Graniczny, M., Kowalski, Z., Chełmiński, J., Czarniak, P., Stępień, U., Czapowski, G., 2019. Monitoring geodynamiczny w zakresie interferometrii satelitarnej pasa wysadów solnych w Polsce oraz próba określenia ruchliwości soli w czwartorzędzie z wykorzystaniem tomografii elektrooporowej i technik modelowania 3D, Raport Końcowy (in Polish). Polish Geological Insitute – NRI, Warsaw 2019. Material effect from the implementation of a task within the scope of the national geological service, agreement no. 913/2014/Wn-07/FG-GO-DN/D from 23.12.2014r.

Poland, M.P., Zebker, H.A., 2022. Volcano geodesy using InSAR in 2020: the past and next decades. Bulletin of Volcanology, **84**: 27; https://doi.org/10.1007/s00445-022-01531-1

Polanin, P., 2017. Monitoring of ground deformation by use aerial laser scanning illustrated with the example of the city of Bytom (in Polish with English summary). Przegląd Górniczy, **73**: 22–30.

Przyłucka, M., 2017. Geostatistical analysis of vertical ground displacements identified by satellite interferometry in the Upper Silesian Coal Basin (in Polish with English summary). Przegląd Górniczy, **73**: 9–17.

Przyłucka, M., Graniczny, M., 2015. Comprehensive use of InSAR and PSInSAR in the study of vertical ground movements in selected regions of the GOP (in Polish with English summary). Przegląd Górniczy, **71**: 80–88.

Przyłucka, M., Graniczny, M., Herrera, G., 2014. Investigating Strong Mining-Induced Ground Subsidence With X-Band SAR Interferometry In Upper Silesia In Poland. Proceedings 5th EARSeL Workshop on Remote Sensing and Geology Surveying the GEOsphere: 104–109.

Przyłucka, M., Herrera, G., Graniczny, M., Colombo, D., Béjar-Pizarro, M., 2015. Combination of conventional and advanced DInSAR to monitor very fast mining subsidence with TerraSAR-X data: Bytom City (Poland). Remote Sensing, **7**: 5300–5328; https://doi.org/10.3390/rs70505300

Przyłucka, M., Kowalski, Z., Perski, Z., 2022. Twenty years of coal mining-induced subsidence in the Upper Silesia in Poland identified using InSAR. International Journal of Coal Science & Technology, **9**: 1–11; https://doi.org/10.1007/s40789-022-00541-w

Ramirez, R.A., Kwon, T.H., 2022. Sentinel-1 persistent scatterer interferometric synthetic aperture radar (PS-InSAR) for long-term remote monitoring of ground subsidence: a case study of a Port in Busan, South Korea. KSCE Journal of Civil Engineering, **26**: 4317–4329; https://doi.org/10.1007/s12205-022-1005-5

Raspini, F., Caleca, F., Del Soldato, M., Festa, D., Confuorto, P., Bianchini, S., 2022. Review of satellite radar interferometry for subsidence analysis. Earth-Science Reviews, **235**: 104239; https://doi.org/10.1016/j.earscirev.2022.104239

Solari, L., Del Soldato, M., Raspini, F., Barra, A., Bianchini, S., Confuorto, P., et al., 2020. Review of satellite interferometry for landslide detection in Italy. Remote Sensing, **12:** 1351; https://doi.org/10.3390/rs12081351

Sopata, P., Stoch, T., Wójcik, A., Mrocheń, D., 2020. Land surface subsidence due to mining-induced tremors in the Upper Silesian Coal Basin (Poland) – case study. Remote Sensing, **12:** 3923; https://doi.org/10.3390/rs12233923

Strozik, G., 2016. Occurrence and influence assessment of mine rooms and galleries on ground surface (in Polish with English summary). Zeszyty Naukowe Wyższej Szkoły Technicznej w Katowicach, **8:** 151–168.

Szuflicki, M., Malon, A., Tymińsk, M., (ed.), 2022. Bilans perspektywicznych zasobów kopalin Polski wg stanu na 31.12. 2021 r. (in Polish). Państwowy Instytut Geologiczny – Państwowy Instytut Badawczy, Warszawa. ISSN 229-4459.

Witkowski, W., Mrocheń, D., Sopata, P., Stoch, T., 2021. Integration of the leveling observations and PSInSAR results for monitoring deformations caused by underground mining. 2021 IEEE International Geoscience and Remote Sensing Symposium IGARSS: 6614–6617; https://doi.org/10.1109/IGARSS47720.2021.9553988

Wu, S., Le, Y., Zhang, L., Ding, X., 2020. Multi-temporal InSAR for urban deformation monitoring: progress and challenges. Journal of Radars**, 9:** 277–294; https://doi.org/10.12000/JR20037

Yun, Y., Lü, X., Fu, X., Xue, F., 2020. Application of spaceborne interferometric synthetic aperture radar to geohazard monitoring. Journal of Radars, **9**: 73–85; https://doi.org/10.12000/JR20007

Zhang, L., Ge, D., Guo, X., Liu, B., Li, M., Wang, Y., 2020. InSAR monitoring surface deformation induced by underground mining using Sentinel-1 images. Proceedings of the International Association of Hydrological Sciences, **382**: 237–240; https://doi.org/10.5194/piahs-382-237-2020